

A Fast and Robust Level Set Method for Image Segmentation Using Fuzzy Clustering and Lattice Boltzmann Method

Souleymane Balla-Arabé, Xinbo Gao, *Senior Member, IEEE*, and Bin Wang

Abstract—In the last decades, due to the development of the parallel programming, the lattice Boltzmann method (LBM) has attracted much attention as a fast alternative approach for solving partial differential equations. In this paper, we first designed an energy functional based on the fuzzy c -means objective function which incorporates the bias field that accounts for the intensity inhomogeneity of the real-world image. Using the gradient descent method, we obtained the corresponding level set equation from which we deduce a fuzzy external force for the LBM solver based on the model by Zhao. The method is fast, robust against noise, independent to the position of the initial contour, effective in the presence of intensity inhomogeneity, highly parallelizable and can detect objects with or without edges. Experiments on medical and real-world images demonstrate the performance of the proposed method in terms of speed and efficiency.

Index Terms—Fuzzy c -means (FCM), image segmentation, intensity inhomogeneity, lattice Boltzmann method (LBM), level set equation (LSE), partial differential equation (PDE).

I. INTRODUCTION

IN COMPUTER vision, image segmentation [38]–[40] is a major and nontrivial task which aims to partition a given image into several regions or to detect an object of interest from the background. This task is more challenging than most of the actual imaging devices produce images corrupted by intensity inhomogeneity. The level set method (LSM) is a part of the whole family of active contour methods (ACMs). The key idea that started the level set fanfare was the Hamilton–Jacobi approach, i.e., a time-dependent equation for a moving surface. This was first done in the seminal work of Osher and Sethian [1]. In 2-D space, the LSM represents a closed curve in the plane as the zero level set of a 3-D function ϕ . For instance,

starting with a curve around the object to be detected, the curve moves toward its interior normal and has to stop on the boundary of the object. Two approaches are usually used to stop the evolving curve on the boundary of the desired object; the first one uses an edge indicator depending on the gradient of the image like in classical snakes and ACMs [2]–[5], [21], [31], and the second one uses some regional attributes to stop the evolving curve on the actual boundary [22], [23], [32] where the authors extend the representative region-based level set from scalar to tensors by simultaneously taking into account the pixel’s gray level and some local statistics such as gradient and orientation. The latter is more robust against noise and can detect objects without edges. One of the most interesting approaches was done in [6] where Chan and Vese introduced a level set formulation to minimize the Mumford and Shah functional [24] that converted the problem into a mean curvature flow problem just like the active contours, but the results outperformed the classical active contours because the stopping term did not depend on the gradient of the image which reduces the dependence on clear edges. However, the method is sensitive to the position of the initial contour, and the evolving curve can be trapped into local minima. In addition, the Chan–Vese (CV) method is not suitable for parallel programming because, at each iteration, the average intensities inside and outside the contour should be computed, which increases drastically the CPU time by increasing communications between processors. For this purpose, we propose a new method which tries to overcome the aforementioned drawbacks. Our method is based on a new idea which aims to stop the evolving curve according to the membership degree of the current pixel to be inside or outside of the active contour. This is done with the help of the modified fuzzy C -means (FCM) objective function obtained in [19] which also takes into consideration the shading image due to the intensity inhomogeneity.

In the LSM, the movement of the zero level set is actually driven by the level set equation (LSE), which is a partial differential equation (PDE). For solving the LSE, most classical methods such as the upwind scheme are based on some finite difference, finite volume or finite element approximations and an explicit computation of the curvature [20]. Unfortunately, these methods cost a lot of CPU time.

Recently, the lattice Boltzmann method (LBM) has been used as an alternative approach for solving LSE [12], [14], [29], [36]. It can better handle the problem of time consuming because the curvature is implicitly computed and the algorithm is simple and highly parallelizable.

Manuscript received December 15, 2011; revised May 4, 2012 and August 27, 2012; accepted August 30, 2012. This work was supported in part by the National Natural Science Foundation of China under Grants 61125204, 61172146, 41031064, 60832005, and 61201293, by the Fundamental Research Funds for the Central Universities, by the Ph.D. Programs Foundation of Ministry of Education of China under Grant 20090203110002, and by the Ocean Public Welfare Scientific Research Project, State Oceanic Administration People’s Republic of China, under Grant 201005017. This paper was recommended by Associate Editor I. Bloch.

S. Balla-Arabé is with the State Key Laboratory of Integrated Services Networks, Xidian University, Xi’an 710071, China (e-mail: balla_arabe_souleymane@yahoo.fr).

X. Gao and B. Wang are with the Video & Image Processing System Laboratory, School of Electronic Engineering, Xidian University, Xi’an 710071, China (e-mail: xbgao@mail.xidian.edu.cn; bwang@xidian.edu.cn).

Color versions of one or more of the figures in this paper are available online at <http://ieeexplore.ieee.org>.

Digital Object Identifier 10.1109/TSMCB.2012.2218233

In this paper, the LBM is used to solve the LSE. The proposed method is based on the approach of the LBM PDE solver defined in [14]. In our proposed method, using a modified FCM objective function, we design a new fuzzy external force (FEF). The method is fast, robust against noise, and efficient whatever the position or the shape of the initial contour and can detect efficiently objects with or without edges. It has, first, the advantage of the FCM which gives it the latitude to stop the evolving curve according to the membership degree of the current pixel, second, the advantages of the LSM which allow it to handle complex shapes, topological changes, and different constraints on the contour smoothness, speed, size, and shape which are easily specified, and, third, the advantages of the LBM which make it very suitable for parallel programming due to its local and explicit nature.

The rest of this paper is organized as follows. In Section II, a general overview of the LSM and the LBM models is presented. In Section III, we explain the formulation of the proposed method. Section IV validates the proposed method through experimental results. Section V concludes this paper.

II. BACKGROUND

The proposed method uses mainly two techniques belonging to different frameworks: the LSM and the LBM.

A. LSM

The LSM is a numerical technique for tracking interfaces and shapes. Using an implicit representation of active contours, it has the advantage of handling automatically topological changes of the tracked shape. In 2-D image segmentation, the LSM represents a closed curve as the zero level set of ϕ , called the level set function. The evolution of the curve starts from an arbitrary starting contour and evolves itself driven by the LSE which can be seen as a convection–diffusion equation

$$\frac{\partial \theta}{\partial t} + \vec{V} \cdot \nabla \phi = b \Delta \phi \quad (1)$$

where $\nabla \phi$ and $\Delta \phi$ are the gradient and the Laplacian of ϕ , respectively. The term $b \Delta \phi$ is called artificial viscosity (Sethian suggested replacing it with $bk|\nabla \phi|$ which is better for handling the evolution of lower dimensional interfaces [12]), and k is the curvature of the distance function ϕ . The LSE can therefore be written as

$$\frac{\partial \theta}{\partial t} + \vec{V} \cdot \nabla \phi = bk|\Delta \phi|. \quad (2)$$

Being an alternative method for solving PDE, the LBM has several advantages, such as parallelizability and simplicity. In this paper, we use the D2Q9 LBM model to resolve the LSE in 2-D space.

B. LBM

The LBM is a numerical framework for modeling Boltzmann particle dynamics on a 2-D or 3-D lattice [13]. It was first designed to solve macroscopic fluid dynamics problems [14]. The method is second order accurate both in time and in

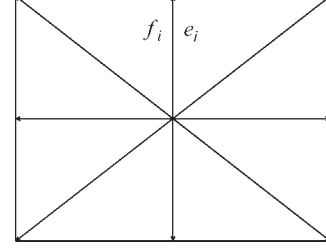


Fig. 1. Spatial structure of the D2Q9 LBM lattice.

space, and in the limit of zero time step and lattice spacing, it yields the Navier–Stokes equations for an incompressible fluid [15].

The proposed method uses the D2Q9 (2-D with eight links with its neighbors and one link for the cell itself) LBM lattice structure. Fig. 1 shows a typical D2Q9 model. Each link has its velocity vector $e_i(\vec{r}, t)$ and the particle distribution $f_i(\vec{r}, t)$ that moves along this link, where \vec{r} is the position of the cell and t is the time. The LBM evolution equation can be written as follows using the Bhatnagar, Gross, and Krook collision model [7]

$$f_i(\vec{r} + \vec{e}_i, t + 1) = f_i(\vec{r}, t) + \frac{1}{\tau} [f_i^{\text{eq}}(\vec{r}, t) - f_i(\vec{r}, t)] \quad (3)$$

where τ represents the relaxation time determining the kinematic viscosity ϑ of the fluid by

$$\vartheta = \frac{1}{3} \left(\tau - \frac{1}{2} \right) \quad (4)$$

and f_i^{eq} is the equilibrium particle distribution defined as

$$f_i^{\text{eq}}(\rho, \vec{u}) = \rho (A_i + B_i(\vec{e}_i \cdot \vec{u}) + C_i(\vec{e}_i \cdot \vec{u})^2 + D_i(\vec{u})^2) \quad (5)$$

where A_i to D_i are constant coefficients depending on the geometry of the lattice links and ρ and \vec{u} are the macroscopic fluid density and velocity, respectively, computed from the particle distributions as

$$\rho = \sum_i f_i \quad \vec{u} = \frac{1}{\rho} \sum_i f_i \vec{e}_i. \quad (6)$$

For modeling typical diffusion computations, the equilibrium function can be simplified as follows [14]:

$$f_i^{\text{eq}}(\rho, \vec{u}) = \rho A_i. \quad (7)$$

In the case of D2Q9 model, $A_i = 4/9$ for the zero link, $A_i = 1/9$ for the axial links, and $A_i = 1/36$ for the diagonal links. Now, the relaxation time τ is determined by the diffusion coefficient γ defined as

$$\gamma = \frac{2}{9}(2\tau - 1). \quad (8)$$

As shown in [14], LBM can be used to solve the parabolic diffusion equation which can be recovered by the Chapman–Enskog expansion

$$\frac{\partial \rho}{\partial t} = \gamma \nabla \cdot \nabla \rho. \quad (9)$$

In this case, the external force can be included as follows:

$$f_i \leftarrow f_i + \frac{2\tau - 1}{2\tau} B_i(\vec{F} \cdot \vec{e}_i). \quad (10)$$

Moreover, thus, (9) becomes

$$\frac{\partial \rho}{\partial t} = \gamma \nabla \cdot \nabla \rho + F. \quad (11)$$

Replacing ρ by the signed distance function ϕ , the LSE can be recovered.

III. PROPOSED METHOD

This section details first the conception of the FCM-based energy function from which we deduce the corresponding LSE. We then set the FEF. Moreover, finally, we implement the proposed method.

A. Energy Function Design

In the image segmentation context, the standard FCM algorithm is an optimization problem for partitioning an image of N pixels, $X = \{x_i\}_{i=1}^N$, into c classes. It aims to minimize a clustering criterion as [7]

$$J(U, V, X) = \sum_{k=1}^c \sum_{i=1}^N u_{ki}^p \|x_i - v_k\|^2$$

$$\text{s.t. } \sum_{k=1}^c u_{ki} = 1 \quad \forall i \quad 0 \leq u_{ki} \leq 1 \quad \forall k, i \quad (12)$$

where U is the *partition matrix* whose element u_{ki} is the *membership* of the i th voxel for k th class. V is the *centroid* vector whose element v_k is the centroid (or prototype) of k th class. The parameter p , called *fuzzy index*, is a weighting exponent on each fuzzy membership and determines the amount of ‘‘fuzziness’’ of the resulting partition. The norm operator $\|\cdot\|$ represents the standard Euclidean distance. The objective function J is minimized when high membership values are assigned to the pixels whose intensities are close to the centroid of its particular class and low membership values are assigned to the pixels whose intensities are far from the centroid.

As done in [7], the bias field is incorporated into the FCM framework by modeling the observed image as follows:

$$Y_i = X_i G_i \quad \forall i \in \{1, 2, \dots, N\} \quad (13)$$

where Y_i , X_i , and G_i are the observed intensity, true intensity, and *gain* field at the i th pixel, respectively. N is the total number of pixels in the magnetic resonance image. The artifact can be modeled as an additive *bias* field by applying a logarithmic transformation to both sides of (13) [7], [8]

$$y_i = x_i + \beta_i \quad \forall i \in \{1, 2, \dots, N\} \quad (14)$$

where y_i and x_i are the observed and true log-transformed intensities at the i th voxel, respectively, and β_i is the bias field at the i th voxel. By incorporating the bias field model into an FCM framework, we will be able to iteratively estimate both the true intensity and the bias field from the observed intensity. By

substituting (14) into (12), the clustering criterion to minimize in the presence of bias field becomes a constrained optimization problem

$$J(U, V, B, Y) = \sum_{k=1}^c \sum_{i=1}^N u_{ki}^p \|y_i - \beta_i - v_k\|^2$$

$$\text{s.t. } \sum_{k=1}^c u_{ki} = 1 \quad \forall i \quad 0 \leq u_{ki} \leq 1 \quad \forall k, i \quad (15)$$

where $Y = \{y_i\}_{i=1}^N$ is the observed image and $B = \{\beta_i\}_{i=1}^N$ is the bias field image.

In a continuous form, the aforementioned criterion can be written as

$$J(U, V, B, Y)$$

$$= \sum_{k=1}^c \int_{\Omega_k} U_k^p(x, y) \|Y(x, y) - B(x, y) - v_k\|^2 dx dy$$

$$\text{s.t. } \sum_{k=1}^c U_k(x, y)$$

$$= 1 \quad \forall x, y \quad 0 \leq U_k(x, y) \leq 1 \quad \forall k, x, y. \quad (16)$$

Consider the two-phase level set although the method can be easily extended to more than two phases. The image domain Ω is segmented into two disjoint regions Ω_1 and Ω_2 , i.e., $c = 2$. In this case, we can introduce a level set function as follows:

$$J(U, V, B, Y, \phi)$$

$$= \int_{\Omega} U_1^p(x, y) \|Y(x, y) - B(x, y) - v_1\|^2 H(\phi) dx dy$$

$$+ \int_{\Omega} U_2^p(x, y) \|Y(x, y) - B(x, y) - v_2\|^2 (1 - H(\phi)) dx dy$$

$$\text{s.t. } U_1(x, y) + U_2(x, y)$$

$$= 1 \quad \forall x, y \quad 0 \leq U_k(x, y) \leq 1 \quad \forall k, x, y \quad (17)$$

where ϕ is a signed distant function. The aforementioned term $J(U, V, B, Y, \phi)$ is used as the data link in our energy functional which is defined as follows:

$$E(U, V, B, Y, \phi) = J(U, V, B, Y, \phi) + \nu |C| \quad (18)$$

where $\nu |C|$ is a regularization term with $\nu > 0$ being a fixed parameter and C being a given curve which is represented implicitly as the zero level of ϕ and $|C|$ is the length of C and can be expressed by the following equation [9]

$$|C| = \int_{\Omega} |\nabla H(\phi)| dx dy. \quad (19)$$

B. LSE

As done in [10], to obtain the LSE, we minimize $E(U, V, B, Y, \phi)$ with respect to ϕ . For fixed U , V , and B , we

use the gradient descent method

$$\frac{\partial \phi}{\partial t} = -\frac{\partial E}{\partial \phi} \quad (20)$$

where $\partial E/\partial \phi$ is the Gâteaux derivative [11] of E . We obtain the following LSE:

$$\begin{aligned} \frac{\partial \phi}{\partial t} &= \delta(\phi) \left(U_1^p(x, y) \|Y(x, y) - B(x, y) - v_1\|^2 \right. \\ &\quad \left. - U_2^p(x, y) \|Y(x, y) - B(x, y) - v_2\|^2 \right) \\ &\quad + \nu \delta(\phi) \operatorname{div} \left(\frac{\nabla \phi}{|\nabla \phi|} \right) \\ \text{s.t. } U_1(x, y) + U_2(x, y) &= 1 \quad \forall x, y \\ 0 \leq U_k(x, y) &\leq 1 \quad \forall k, x, y. \end{aligned} \quad (21)$$

However, for solving the minimization problem of $E(U, V, B, Y, \phi)$, we should also compute the first derivatives of $E(U, V, B, Y, \phi)$ with respect to u_{ki} , v_k , and β_i and set them equal to zero. We thus obtain three necessary conditions

$$U_k^*(x, y) = \frac{1}{\sum_{l=1}^c \left(\frac{\|Y(x, y) - B(x, y) - v_l\|}{\|Y(x, y) - B(x, y) - v_k\|} \right)^{\frac{2}{p-1}}} \quad (22)$$

$$v_k^* = \frac{\int_{\Omega} U_k^p(x, y) (Y(x, y) - B(x, y)) dx dy}{\int_{\Omega} U_k^p(x, y) dx dy} \quad (23)$$

$$B^*(x, y) = Y(x, y) - \frac{\sum_{k=1}^c U_k^p(x, y) v_k}{\sum_{k=1}^c U_k^p(x, y)}. \quad (24)$$

C. Lattice Boltzmann Solver for LSE

By using the gradient projection method of Rosen [17], we can replace $\delta(\phi)$ by $|\nabla \phi|$ in the proposed LSE, and as ϕ is a distance function, we have $|\nabla \phi| = 1$ [16], [20] and will stay at each step since an adaptive approach is not used and the distant field is valid in the whole domain [25]. Thus, the proposed LSE becomes

$$\begin{aligned} \frac{\partial \phi}{\partial t} &= U_1^p(x, y) \|Y(x, y) - B(x, y) - v_1\|^2 \\ &\quad - U_2^p(x, y) \|Y(x, y) - B(x, y) - v_2\|^2 + \nu \operatorname{div}(\nabla \phi) \\ \text{s.t. } U_1(x, y) + U_2(x, y) &= 1 \quad \forall x, y \\ 0 \leq U_k(x, y) &\leq 1 \quad \forall k, x, y. \end{aligned} \quad (25)$$

Replacing ρ by the signed distance function ϕ , (11) becomes

$$\frac{\partial \phi}{\partial t} = \gamma \operatorname{div}(\nabla \phi) + F. \quad (26)$$

By setting the external force

$$\begin{aligned} F &= \lambda \left(U_1^p(x, y) \|Y(x, y) - B(x, y) - v_1\|^2 \right. \\ &\quad \left. - U_2^p(x, y) \|Y(x, y) - B(x, y) - v_2\|^2 \right) \end{aligned} \quad (27)$$

where λ is a positive parameter; we can see that (25) is only a variational formula of (26) and, thus, can be solved by the LBM with the above-defined FEF. The choice of parameter p is at great importance for the segmentation result. Different values for p will result in the different results, as following.

- 1) If $p > 2$, then the exponent $2/(p-1)$ in (22) decreases the membership value of the pixels that are closed to the centroid. The segmentation result will therefore be wrong since it is intuitively better that the membership value be high for those pixels who are closed to the centroid.
- 2) If $p \rightarrow \infty$, all the membership values tend to $1/c$. This implies that the

$$\begin{aligned} \text{FEF} &\rightarrow \lambda \left(\left(\frac{1}{c} \right)^p \|Y(x, y) - B(x, y) - v_1\|^2 \right. \\ &\quad \left. - \left(\frac{1}{c} \right)^p \|Y(x, y) - B(x, y) - v_2\|^2 \right) \rightarrow 0. \end{aligned}$$

There is, therefore, no link with the image data in the LSM process. Therefore, segmentation is impossible.

- 3) If $p \rightarrow 1$, the exponent $2/(p-1)$ increases the membership values of the pixels who are closed to the centroid. As $p \rightarrow 1$, the membership tends to one for the closest pixels and tends to zero for all the other pixels. This case is equivalent to the use of the k -means objective function instead of the FCM one. The segmentation is therefore rigid, and we lose the advantage of FCM over k -means.

For all these reasons, a suitable choice of the parameter p can be the value of two, which is therefore used in all our experiments.

D. Implementation

When using LBM to resolve the convection–diffusion equation, the particle density is set as ϕ which is a signed distance function. Since the particle number of the cell cannot be negative, we modify the distance function as $\phi' = \phi - \min(\phi)$. The contour is those pixels which satisfy $\phi' = -\min(\phi)$.

The steps for the computation are outlined as follows.

- 1) Initialize the distance function ϕ and class centroid values v_1 and v_2 . Initialize B with zeros.
- 2) Compute $U_1^p(x, y)$ and $U_2^p(x, y)$ with (22).
- 3) Compute v_1 and v_2 with (23).
- 4) Compute B with (24).
- 5) Compute the external force with (27).
- 6) Include the external force based on (10).
- 7) Resolve the convection–diffusion equation with LBM with (3).
- 8) Accumulate the $f_i(\vec{r}, t)$ values at each grid point by (6), which generates an updated distance value at each point.
- 9) Find the contour.
- 10) If the segmentation is not done, increase the value of λ and go back to step 5).

We should notice that the B obtained from (24) is a “residual” image but not necessarily the bias field image [7]. In [18], the adaptive fuzzy c -means (AFCM) algorithm by Pham and Prince solved the problem by introducing regularization terms

into the objective function that ensure the resulted bias field image to be smooth. The regularization terms, however, make the estimation of the bias field a computationally intensive process. As done in [7], another solution is to estimate the bias field by filtering the residual image B in (24) using an iterative low-pass spatial filter. This filtering strategy is based on the fact that the bias field is of low spatial frequency and the assumption that other components in the residual image are of higher frequency.

IV. EXPERIMENTS AND ANALYSIS

This section is divided into three parts. The first part demonstrates the accuracy and the effectiveness of the proposed method by comparing it with four level set image segmentation methods [10], [12], [25], [37]. The second part illustrates the ability of the proposed method in terms of speed and efficiency. The third part evaluates objectively our method using the supervised Hausdorff method and the global consistency error (GCE) by Martin. In the implementation of our method, the value of the *fuzzy index* p is set to two, the class centroid values v_1 and v_2 are randomly initialized at zero and one, respectively, and the diffusion coefficient γ is set to 15. All the methods have been implemented using Matlab R2010b installed on a PC Advanced Micro Devices (AMD) Athlon [trademark (tm)] 5200 processor with a clock speed of 2.31 GHz and 2 GB of RAM.

A. Comparison in Terms of Effectiveness and Accuracy

In this part, we compare the proposed method with four level set image segmentation methods of which three are LBM based. The first one was introduced by Hagan and Zhao in [25] for 3-D image segmentation, the second one was introduced by Chen *et al.* in [12], the third one was introduced by Li *et al.* in [10], and the last one was introduced by Wang *et al.* in [37].

Fig. 2 shows the proposed method on Magnetic Resonance Imaging (MRI) image of the knee. Intensity inhomogeneities can be clearly seen in the image. Fig. 2(a) shows the initial contour, Fig. 2(b) shows the segmentation result using the method by Chen *et al.*, Fig. 2(c) shows the segmentation result using the method by Hagan and Zhao, Fig. 2(d) shows the segmentation result using the method introduced by Wang *et al.*, Fig. 2(e) shows the segmentation result using the method by Li *et al.*, and Fig. 2(f) shows the segmentation result using the proposed method.

We can see that the proposed method gives the best segmentation results whatever the shape and the position of the initial contour and the resulting contours are thin and present no discontinuities. This allows it to be efficient in automatic systems. The method by Chen *et al.* and the method by Li *et al.* both based on an edge stopped function fail because the objects in the image have weak edges. The method by Hagan and Zhao is handicapped by intensity inhomogeneity and tends to give an oversegmented result; furthermore, the resulting contours present many discontinuities. The method by Wang *et al.* gives a different result according to the initial contour; it is therefore less robust than the proposed method, and furthermore, the quality of the segmentation using the proposed method is better.

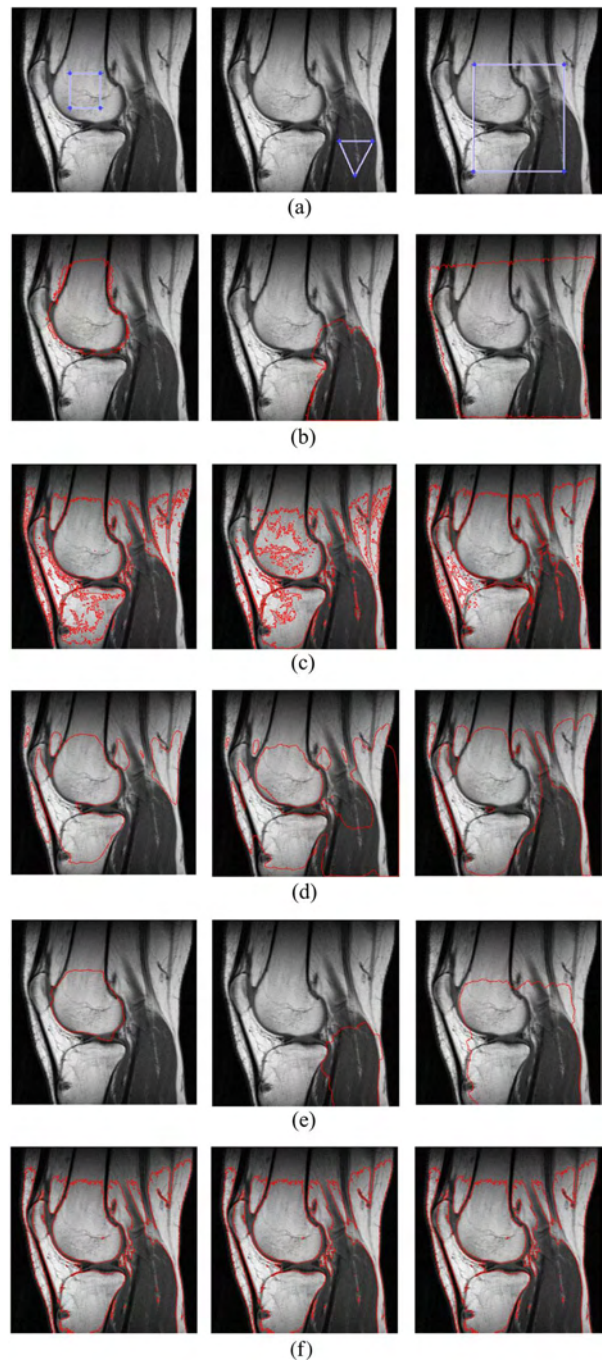


Fig. 2. Segmentation of an MRI image of the knee. (a) shows the initial contours, (b) shows the segmentation results of the method by Chen *et al.*, (c) shows the segmentation results of the method by Hagan and Zhao, (d) shows the segmentation results of the method introduced by Wang *et al.*, (e) shows the segmentation results of the method by Li *et al.*, and (f) shows the segmentation result of the proposed method.

Fig. 3 shows the segmentation result of an MRI image of the knee corrupted by a multiplicative noise. We used the Matlab speckle function with $v = 0.04$ to insert the multiplicative noise. It can be seen that the proposed method is more robust to noise and gives the best results.

Fig. 4 shows the segmentation result of an MRI image of blood vessels. The result of the proposed method is clearer and is not oversegmented like, for example, that of method by Hagan and Zhao; furthermore, the resulting contours

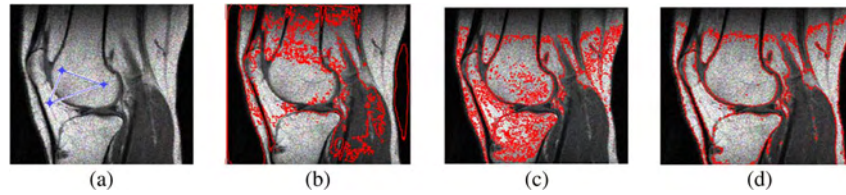


Fig. 3. Segmentation of an MRI image of the knee corrupted by a multiplicative noise. (a) Initial contour. (b) Segmentation result using the method by Chen *et al.* (c) Segmentation result using the method by Hagan and Zhao. (d) Segmentation result using the proposed method.

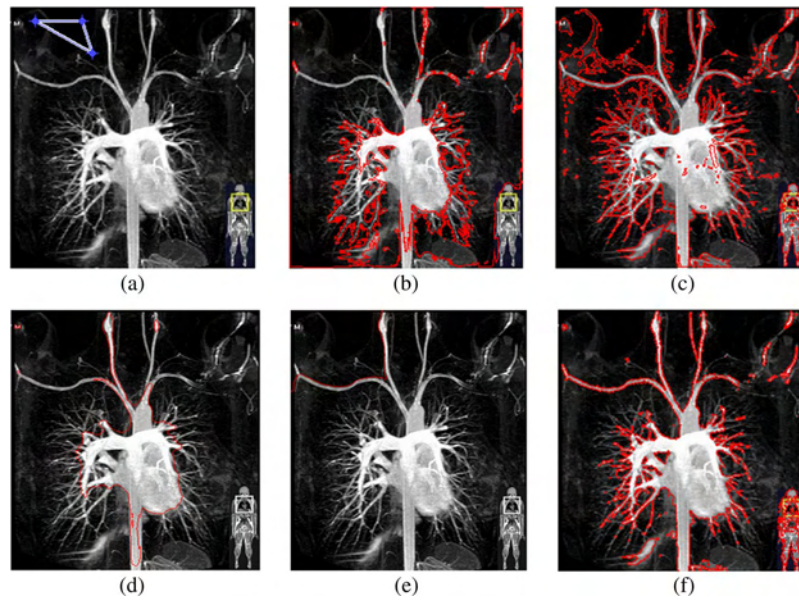


Fig. 4. Segmentation of an MRI image of blood vessels. (a) Initial contour. (b) Segmentation result using the method by Chen *et al.* (c) Segmentation result using the method by Hagan and Zhao. (d) Segmentation result using the method introduced by Wang *et al.* (e) Segmentation result using the method by Li *et al.* (f) Segmentation result using the proposed method.

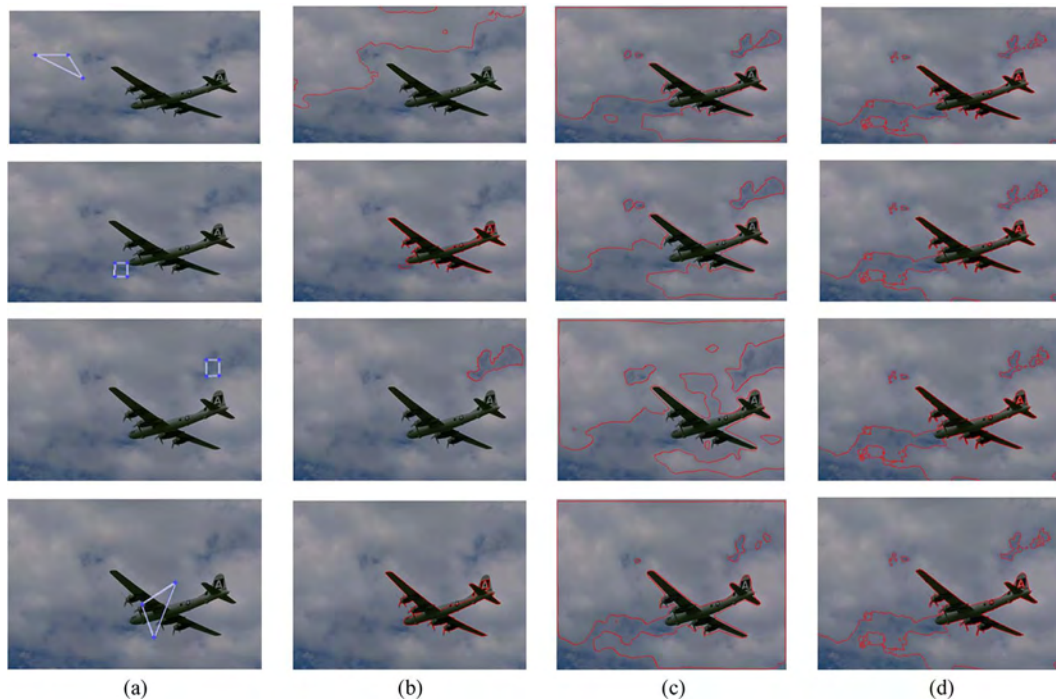


Fig. 5. (a) Initial contours. (b) Segmentation results of the CV method. (c) Segmentation results of the Gibou-Fedkiw method. (d) Segmentation results of the proposed method.

TABLE I
CPU TIMES OF THE EXPERIMENT SHOWN IN FIG. 5

Methods	Initial Contour I	Initial Contour II	Initial Contour III	Initial Contour IV
	CPU time (s)			
Proposed Method	0.79	0.78	0.77	0.7296
Chan-Vese	164.36	93.28	94.83	102.7410
Gibou-Fedkiw	0.39	0.39	0.37	0.3843
Image dimensions 481 X 321				

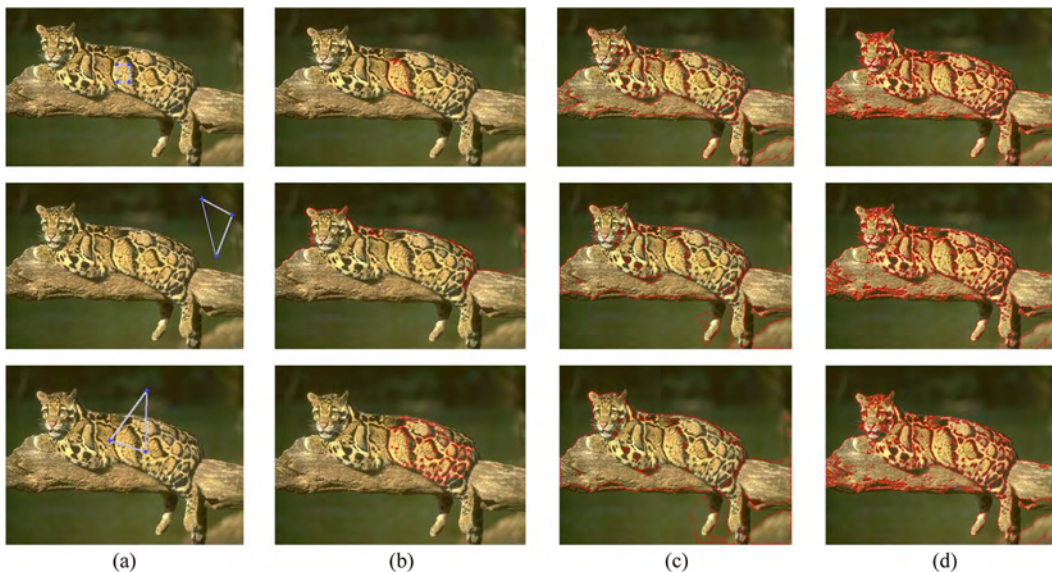


Fig. 6. (a) Initial contours. (b) Segmentation results of the CV method. (c) Segmentation results of the Gibou–Fedkiw method. (d) Segmentation results of the proposed method.

TABLE II
CPU TIMES OF THE EXPERIMENT SHOWN IN FIG. 6

Methods	Initial Contour I	Initial Contour II	Initial Contour III
	CPU time (s)		
Proposed Method	0.92	0.93	0.9554
Chan-Vese	94.42	183.29	112.3841
Gibou-Fedkiw	0.41	0.39	0.4803
Image dimensions 481 X 321			

are closed and present nondiscontinuities. The method by Wang *et al.* gives again an undersegmented result, and in the method by Li *et al.*, the contour is trapped in a local minimum.

B. Comparison in Terms of Speed and Efficiency

In this part, we compare the proposed method with the well-known CV method [6] and the fast Gibou–Fedkiw method described in [26].

Fig. 5 shows the segmentation result obtained on a real-world image with different initial contours. All the CPU times are displayed in Table I. In terms of quality and accuracy, it can be seen that the proposed method gives better result than the Gibou–Fedkiw method whatever the shape and the position of the initial contour. The Gibou–Fedkiw method cannot detect steep corners and has all the inconveniences of k -means algorithm, i.e., the result changes with the initial contour and

one should run the algorithm several times in order to choose the best result; thus, this method cannot be used in automatic systems, and even if it is fast when running it one time, the segmentation will take more much time since one should run the method several times. We can also remark that the proposed method can give better results than the CV method and can detect all the contours whatever the position of initial contour, while in the CV method, the contour can be trapped in a local minimum. Furthermore, the proposed method is more than 100 times faster than the CV method and can be faster when implemented on graphics processing unit (GPU) due to the local and explicit nature of the LBM solver.

Fig. 6 shows also the segmentation result obtained on a real-world image with different initial contours. The CPU times are displayed in Table II. The proposed method gives better result than the CV and Gibou–Fedkiw methods whatever the shape and the position of the initial contour. We can also remark that

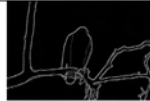
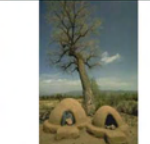
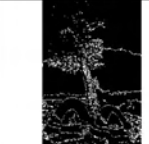
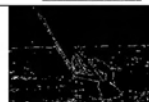
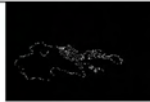
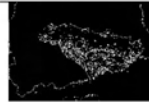
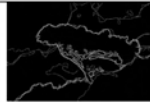
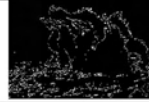
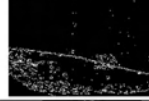
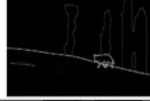
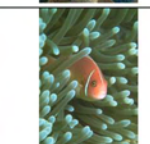
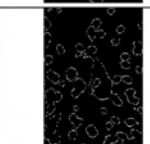
	Test images	Chan- Vese	Gabou- Fedkiw	Proposed method	Humans
1					
2					
3					
4					
5					
6					
7					
8					
9					
10					
11					
12					
13					
14					
	(a)	(b)	(c)	(d)	(e)

Fig. 7. (a) Original images. (b) Segmentation results using the CV method. (c) Segmentation results using the Gibou–Fedkiw method. (d) Segmentation results using the proposed method. (e) Segmentations did by humans.

TABLE III
RESULTS OF THE QUALITATIVE EVALUATION BETWEEN THE PROPOSED METHOD, THE CV METHOD, AND THE FAST GIBOU–FEDKIW METHOD

Test images	Hausdorff's criterion			Martin's criterion		
	Proposed method	Chan-Vese method	Gibou method	Proposed method	Chan-Vese method	Gibou method
1	14641	41697	20025	0.0726	0.0764	0.0735
2	11252	55777	38809	0.1512	0.1602	0.1616
3	10829	17956	17424	0.0622	0.0632	0.0577
4	4948	27092	18122	0.0923	0.1060	0.1112
5	14452	43621	15337	0.0869	0.0968	0.0891
6	8649	17972	9125	0.1083	0.1397	0.1276
7	17341	15572	42653	0.0255	0.0222	0.0263
8	4306	7157	6089	0.0814	0.0855	0.0844
9	3869	34613	16916	0.1138	0.1292	0.1405
10	2482	36805	3218	0.0849	0.0988	0.1216
11	7489	16465	13577	0.1054	0.1117	0.1061
12	3589	5159	9698	0.0580	0.0602	0.0696
13	10546	21145	10730	0.1068	0.0934	0.0918
14	8117	33597	8164	0.0781	0.0802	0.0991

the result of the Gibou–Fedkiw method changes with the initial contour. The proposed method gives the same good result, while in the CV method, the contour is trapped in a local minimum and it is far faster.

C. Supervised Evaluation of the Proposed Method

In order to objectively evaluate the proposed method, we use two well-known metrics, the Hausdorff distance and the GCE by Martin. As defined in [27] and [28], the Hausdorff distance measures the similarity between two images. The lower it is, the better the segmentation result is. The Hausdorff distance is computed as follows:

$$\text{HAU}(I_C, I_{\text{ref}}) = \max(h(I_C, I_{\text{ref}}), h(I_{\text{ref}}, I_C)) \quad (28)$$

where

$$h(I_C, I_{\text{ref}}) = \max_{a \in I_C} \left(\min_{b \in I_{\text{ref}}} \|a - b\| \right). \quad (29)$$

The metric by Martin measures also the similarity between two images; it is shown to be effective for qualitative similarity comparison between segmentations by humans, which often produce results with different degrees of perceived details, which are all intuitively reasonable and therefore “correct.” There are two variants of the measure by Martin [33]–[35], the GCE and the local consistency error (LCE). Specifically

$$\text{GCE}(I, V) = \frac{1}{A} \min \left\{ \sum_s E(s), \sum_s E'(s) \right\} \quad (30)$$

$$\text{LCE}(R, V) = \frac{1}{A} \sum_s \min \{E(s), E'(s)\} \quad (31)$$

where I is the image, V is the ground truth, R is the segmentation result of the method to evaluate, A is the number of pixels in the image

$$E(s) = \frac{\text{card}\left(\frac{V_j}{R_i}\right)}{\text{card}(V_j)} \quad (32)$$

and

$$E(s) = \frac{\text{card}\left(\frac{V_j}{R_i}\right)}{\text{card}(V_j)} \quad (32)$$

$$E'(s) = \frac{\text{card}\left(\frac{R_i}{V_j}\right)}{\text{card}(R_i)} \quad (33)$$

with V_j as the region of the ground truth to which the pixel s belongs and R_i as the region of the segmented image to which the pixel s belongs. This measure produces a real-valued output in the range of [0, 1] where 0 signifies no error and 1 signifies worst segmentation.

Fig. 7 shows the segmentation results used to quantitatively evaluate the proposed method, the CV method, and the Gibou–Fedkiw method. The images, and the humans’ segmentations used as the ground truth, are from the Berkeley segmentation data set BSDS300 [30]. Table III displays the evaluation results using the metrics by Hausdorff and Martin. We can notice that the proposed method has the lowest values of the criteria by Hausdorff and Martin; thus, its segmentation result is better than those of CV and the Gibou–Fedkiw methods.

V. CONCLUSION

In this paper, we have presented a level set image segmentation method based on the idea of stopping the evolving contour according to the degree of membership of the active pixel to be inside or outside of this evolving contour. It is done with the help of the FCM partition matrix. The LSE is solved by using the powerful, simple, and highly parallelizable LBM which allows the method to be a good candidate for GPU implementation. The method gives promising results. Experimental results on medical and real-world images have demonstrated the good performance of the proposed method in terms of speed, effectiveness in the presence of intensity inhomogeneities, accuracy, robustness against noise, and efficiency whatever the initial contour. Future works can be an implementation of the proposed method using a parallel device such as the GPU in

order to fully take advantage of the LBM. The method will be faster and suitable for 3-D volume image segmentation. The segmentation result can also be enhanced by inserting spatial information in the FEF, but one should be careful to not affect the parallelizability of the method.

REFERENCES

- [1] S. Osher and J. Sethian, "Fronts propagating and curvature dependent speed: Algorithms based on Hamilton–Jacobi formulation," *J. Comput. Phys.*, vol. 79, no. 1, pp. 12–49, Nov. 1988.
- [2] M. Kass, A. Witkin, and D. Terzopoulos, "Snakes: Active contour models," *Int. J. Comput. Vis.*, vol. 1, no. 4, pp. 321–331, Jan. 1988.
- [3] V. Caselles, F. Catté, and F. Dibos, "A geometric model for active contours in image processing," *Numer. Math.*, vol. 66, no. 1, pp. 1–31, 1993.
- [4] R. Malladi, J. Sethian, and B. Vemuri, "A topology independent shape modeling scheme," in *Proc. SPIE Conf. Geometric Methods Comput. Vis. II*, San Diego, CA, 1993, vol. 2031, pp. 246–258.
- [5] V. Caselles, R. Kimmel, and G. Sapiro, "On geodesic active contours," *Int. J. Comput. Vis.*, vol. 22, no. 1, pp. 61–79, 1997.
- [6] T. Chan and L. Vese, "Active contours without edges," *IEEE Trans. Image Process.*, vol. 10, no. 2, pp. 266–277, Feb. 2001.
- [7] W. Chen and M. L. Giger, "A fuzzy c -means (FCM) based algorithm for intensity inhomogeneity correction and segmentation of MR images," in *Proc. IEEE Int. Symp. Biomed. Imaging: Nano Macro*, 2004, vol. 2, pp. 1307–1310.
- [8] W. M. Wells, W. E. Grimson, R. Kikinis, and F. A. Jolesz, "Adaptive segmentation of MRI data," *IEEE Trans. Med. Imag.*, vol. 15, no. 4, pp. 429–442, Aug. 1996.
- [9] L. C. Evans and R. F. Gariepy, *Measure Theory and Fine Properties of Functions*. Boca Raton, FL: CRC Press, 1992.
- [10] C. Li, C. Xu, C. Gui, and M. Fox, "Distance regularized level set evolution and its application to image segmentation," *IEEE Trans. Image Process.*, vol. 19, no. 12, pp. 3243–3254, Dec. 2010.
- [11] G. Aubert and P. Kornprobst, "Mathematical problems in image processing: Partial differential equations and the calculus of variations," in *Applied Mathematical Sciences*, vol. 147. Berlin, Germany: Springer-Verlag, 2001.
- [12] Y. Chen, Z. Yan, and Y. Chu, "Cellular automata based level set method for image segmentation," in *Proc. IEEE/ICME*, Beijing, China, May 2007, pp. 23–27.
- [13] S. Succi, *The Lattice Boltzmann Equation for Fluid Dynamics and Beyond Numerical Mathematics and Scientific Computation*. New York: Oxford Univ. Press, 2001.
- [14] Y. Zhao, "Lattice Boltzmann based PDE solver on the GPU," *Visual Comput.*, vol. 24, no. 5, pp. 323–333, Mar. 2007.
- [15] X. He and L. Luo, "Lattice Boltzmann model for incompressible Navier–Stokes equation," *J. Stat. Phys.*, vol. 88, no. 3/4, pp. 927–944, 1997.
- [16] J. Aujol and G. Aubert, "Signed distance functions and viscosity solutions of discontinuous Hamilton–Jacobi equations," INRIA, Le Chesnay Cedex, France, 2002, inria-00072081, version 1, ref. RR-4507.
- [17] J. G. Rosen, "The gradient projection method for nonlinear programming. II, nonlinear constraints," *J. SIAM*, vol. 9, no. 4, pp. 514–532, Dec. 1961.
- [18] D. L. Pham and J. L. Prince, "Adaptive fuzzy segmentation of magnetic resonance images," *IEEE Trans. Med. Imag.*, vol. 18, no. 9, pp. 737–752, Sep. 1999.
- [19] P. L. Bhatnagar, E. P. Gross, and M. Krook, "A model for collision processes in gases. I. Small amplitude processes in charged and neutral one-component systems," *Phys. Rev.*, vol. 94, no. 3, pp. 511–525, 1954.
- [20] S. Osher and R. Fedkiw, *Level Set Methods and Dynamic Implicit Surfaces*. New York: Springer-Verlag, 2003.
- [21] L. D. Cohen, "On active contour models and balloons," *Comput. Vis., Graph., Image Process.*, vol. 53, no. 2, pp. 211–218, Mar. 1991.
- [22] N. Paragios and R. Deriche, "Geodesic active contours for supervised texture segmentation," in *Proc. IEEE Conf. CVPR*, 1999, pp. I:1034–I:1040.
- [23] R. Ronfard, "Region based strategies for active contour models," *Int. J. Comput. Vis.*, vol. 13, no. 2, pp. 229–251, Oct. 1994.
- [24] D. Mumford and J. Shah, "Optimal approximations by piecewise smooth functions and associated variational problems," *Commun. Pure Appl. Math.*, vol. 42, no. 5, pp. 577–685, Jul. 1989.
- [25] A. Hagan and Y. Zhao, "Parallel 3-D image segmentation of large data set on a GPU cluster," in *Proc. ISVC*, 2009, pp. 960–969.
- [26] F. Gibou and R. Fedkiw, "A fast hybrid k -means level set algorithm for segmentation," in *Proc. 4th Annu. Hawaii Int. Conf. Stat. Math.*, 2005, pp. 281–291.
- [27] M. Bauchemin, K. Thomson, and G. Edwards, "On the Hausdorff distance used for the evaluation of segmentation results," *Can. J. Remote Sens.*, vol. 24, no. 1, pp. 3–8, 1998.
- [28] S. Chabrier, H. Laurent, C. Rosenberger, and B. Emile, "Comparative study of contour detection evaluation criteria based on dissimilarity measures," *EURASIP J. Image Video Process.*, vol. 2008, pp. 693 053–1–693 053–13, Feb. 2008.
- [29] S. Balla-Arabé, B. Wang, and X.-B. Gao, "Level set region based image segmentation using lattice Boltzmann method," in *Proc. 7th Int. Conf. Comput. Intell. Security*, Sanya, China, Dec. 2011, pp. 1159–1163.
- [30] D. Martin, C. Fowlkes, D. Tal, and J. Malik, "A database of human segmented natural images and its application to evaluating segmentation algorithms and measuring ecological statistics," in *Proc. 8th Int. Conf. Comput. Vis.*, Jul. 2001, vol. 2, pp. 416–423.
- [31] X.-B. Gao, B. Wang, D. Tao, and X. Li, "A relay level set method for automatic image segmentation," *IEEE Trans. Syst., Man, Cybern. B, Cybern.*, vol. 41, no. 2, pp. 518–525, Apr. 2011.
- [32] B. Wang, X.-B. Gao, D. Tao, and X. Li, "A unified tensor level set for image segmentation," *IEEE Trans. Syst., Man, Cybern. B, Cybern.*, vol. 40, no. 3, pp. 857–867, Jun. 2010.
- [33] D. R. Martin, "An empirical approach to grouping and segmentation," Ph.D. dissertation, Univ. California, Berkeley, CA, 2002.
- [34] P. Sylvie and G. Laurent, "Evaluation of image segmentation: State of the art, new criteria and comparison," *traitement du signal*, vol. 23, no. 2, pp. 109–124, 2006.
- [35] M. Polak, H. Zhang, and M. Pi, "An evaluation metric for image segmentation of multiple objects," *Image Vis. Comput.*, vol. 27, no. 8, pp. 1223–1227, Jul. 2009.
- [36] S. Balla-Arabé and X. Gao, "Image multi-thresholding by combining the lattice Boltzmann model and a localized level set algorithm," *Neurocomputing*, vol. 93, pp. 106–114, Sep. 2012.
- [37] Z. Wang, Z. Yan, and G. Chen, "Lattice Boltzmann method of active contour for image segmentation," in *Proc. 6th ICIG*, 2011, pp. 338–343.
- [38] J. Ding, R. Ma, J. Yang, and S. Chen, "A tree-structured framework for purifying "complex" clusters with structural roles of individual data," *Pattern Recognit.*, vol. 43, no. 11, pp. 3753–3767, Nov. 2010.
- [39] J. Ding, J. Shen, H. Pang, S. Chen, and J.-Y. Yang, "Exploiting intensity inhomogeneity to extract textured objects from natural scenes," in *Proc. ACCV*, 2009, vol. 3, pp. 1–10.
- [40] P. Arbelaez, M. Maire, C. Fowlkes, and J. Malik, "From contours to regions: An empirical evaluation," in *Proc. CVPR*, 2009, pp. 2294–2301.



Souleymane Balla-Arabé received the M.Eng. degree in electronics from the Polytechnic Military School, Algiers, Algeria, in 2004. He is currently working toward the Ph.D. degree in communication and information engineering in the State Key Laboratory of Integrated Services Networks, Xidian University, Xi'an, China.

His research interests are image segmentation and graphics-processing-unit-based computation.



Xinbo Gao (M'02–SM'07) received the B.Eng., M.Sc., and Ph.D. degrees in signal and information processing from Xidian University, Xi'an, China, in 1994, 1997, and 1999, respectively.

From 1997 to 1998, he was a Research Fellow with the Department of Computer Science, Shizuoka University, Shizuoka, Japan. From 2000 to 2001, he was a Postdoctoral Research Fellow with the Department of Information Engineering, The Chinese University of Hong Kong, Shatin, Hong Kong. Since 2001, he has been with the School of Electronic

Engineering, Xidian University, where he is currently the Professor of pattern recognition and intelligent system and the Director of the Video & Image Processing System Laboratory. His research interests are computational intelligence, machine learning, computer vision, pattern recognition, and wireless communications. In these areas, he has published five books and around 150 technical articles in refereed journals and proceedings including IEEE TRANSACTIONS ON IMAGE PROCESSING, IEEE TRANSACTIONS ON CIRCUITS AND SYSTEMS FOR VIDEO TECHNOLOGY, IEEE TRANSACTIONS ON NEURAL NETWORKS, and IEEE TRANSACTIONS ON SYSTEMS, MAN AND CYBERNETICS, Pattern Recognition, etc. He is on the editorial boards of journals including *EURASIP Signal Processing* (Elsevier) and *Neurocomputing* (Elsevier).

Dr. Gao served as the General Chair/Cochair or Program Committee Chair/Cochair or program committee (PC) member for around 30 major international conferences. He is currently a Fellow of Institution of Engineering and Technology (IET).



Bin Wang received the B.Sc. and M.Sc. degrees in electronics and information system from Northwest University, Xi'an, China, in 1999 and 2002, respectively, and the Ph.D. degree in pattern recognition and intelligent system from Xidian University, Xi'an, in 2010.

He is currently an Associate Professor with the Video & Image Processing System Laboratory, School of Electronic Engineering, Xidian University. His research interest is image segmentation and analysis.